Journal of Low Temperature Physics manuscript No.
(will be inserted by the editor)

Lowering the energy threshold of the CUORE experiment: benefits in the surface alpha events reconstruction

Comparison between optimum trigger and derivative trigger performance in the search for $0\nu\beta\beta$

Alice Campani[1,2] · D.Q. Adams[3] · C.Alduino[3] · K.Alfonso[4] · F.T. Avignone III[3] · O.Azzolini[5] · G. Bari[6] · F. Bellini[7,8] · G. Benato[9] · M. Biassoni[10] · A. Branca[11,10] · C. Brofferio[11,10] · C. Bucci[12] · A. Caminata[2] · L. Canonica[13,12] · X. G. Cao[14] · S. Capelli[11,10] · L. Cappelli[12,9,15] · L. Cardani[8] · P. Carniti[11,10] · N. Casali[8] · D. Chiesa[11,10] · N. Chott[3] · M. Clemenza[11,10] · S. Copello[16,12] · C. Cosmelli[7,8] · O. Cremonesi[10] · R. J. Creswick[3] · A. D'Addabbo[12] · D. D'Aguanno[12,17] · I. Dafinei[8] · C. J. Davis[18] · S. Dell'Oro[19] · S. Di Domizio[1,2] · V. Dompè[12,16] · D. Q. Fang[14] · G. Fantini[12,16] · M. Faverzani[11,10] · E. Ferri[11,10] · F. Ferroni[16,8] · E. Fiorini[10,11] · M. A. Franceschi[20] · S. J. Freedman[15,9⋆] · B. K. Fujikawa[15] · A. Giachero[11,10] · L. Gironi[11,10] · A. Giuliani[21] · P. Gorla[12] · C. Gotti[11,10] · T. D. Gutierrez[22] · K. Han[23] · K. M. Heeger[18] · R. G. Huang[9] · H. Z. Huang[4] · J. Johnston[13] · G. Keppel[5] · Yu. G. Kolomensky[9,15] · C. Ligi[20] · Y. G. Ma[14] · L. Ma[14] · L. Marini[9,15] · R. H. Maruyama[18] · Y. Mei[15] · N. Moggi[24,6] · S. Morganti[8] · T. Napolitano[20] · M. Nastasi[11,10] · J. Nikkel[18] · C. Nones[25] · E. B. Norman[26,27] · V. Novati[21] · A. Nucciotti[11,10] · I. Nutini[11,10] · T. O'Donnell[19] · J. L. Ouellet[13] · C. E.

⋆ Deceased

Pagliarone[12,17] · **L. Pagnanini**[11,10] · **M. Pallavicini**[1,2] · **L. Pattavina**[12] · **M. Pavan**[11,10] · **G. Pessina**[10] · **V. Pettinacci**[8] · **C. Pira**[5] · **S. Pirro**[12] · **S. Pozzi**[11,10] · **E. Previtali**[10] · **A. Puiu**[11,10] · **C. Rosenfeld**[3] · **C. Rusconi**[3,12] · **M. Sakai**[9] · **S. Sangiorgio**[26] · **B. Schmidt**[15] · **N. D. Scielzo**[26] · **V. Sharma**[19] · **V. Singh**[9] · **M. Sisti**[11,10] · **D. Speller**[18] · **L. Taffarello**[28] · **F. Terranova**[11,10] · **C. Tomei**[8] · **M. Vignati**[8] · **S. L. Wagaarachchi**[9,15] · **B. S. Wang**[26,27] · **B. Welliver**[15] · **J. Wilson**[3] · **K. Wilson**[3] · **L. A. Winslow**[13] · **L. Zanotti**[11,10] · **S. Zimmermann**[29] · **S. Zucchelli**[24,6]

Received: date / Accepted: date

E-mail: alice.campani@ge.infn.it

[1]Dipartimento di Fisica, Università di Genova, Genova I-16146, Italy
[2]INFN – Sezione di Genova, Genova I-16146, Italy
[3]Department of Physics and Astronomy, University of South Carolina, Columbia, SC 29208, USA
[4]Department of Physics and Astronomy, University of California, Los Angeles, CA 90095, USA
[5]INFN – Laboratori Nazionali di Legnaro, Legnaro (Padova) I-35020, Italy
[6]INFN – Sezione di Bologna, Bologna I-40127, Italy
[7]Dipartimento di Fisica, Sapienza Università di Roma, Roma I-00185, Italy
[8]INFN – Sezione di Roma, Roma I-00185, Italy
[9]Department of Physics, University of California, Berkeley, CA 94720, USA
[10]INFN – Sezione di Milano Bicocca, Milano I-20126, Italy
[11]Dipartimento di Fisica, Università di Milano-Bicocca, Milano I-20126, Italy
[12]INFN – Laboratori Nazionali del Gran Sasso, Assergi (L'Aquila) I-67100, Italy
[13]Massachusetts Institute of Technology, Cambridge, MA 02139, USA
[14]Shanghai Institute of Applied Physics, Chinese Academy of Sciences, Shanghai 201800, China
[15]Nuclear Science Division, Lawrence Berkeley National Laboratory, Berkeley, CA 94720, USA
[16]INFN – Gran Sasso Science Institute, L'Aquila I-67100, Italy
[17]Dipartimento di Ingegneria Civile e Meccanica, Università degli Studi di Cassino e del Lazio Meridionale, Cassino I-03043, Italy
[18]Wright Laboratory, Department of Physics, Yale University, New Haven, CT 06520, USA
[19]Center for Neutrino Physics, Virginia Polytechnic Institute and State University, Blacksburg, Virginia 24061, USA
[20]INFN – Laboratori Nazionali di Frascati, Frascati (Roma) I-00044, Italy
[21]CSNSM, Univ. Paris-Sud, CNRS/IN2P3, Université Paris-Saclay, 91405 Orsay, France
[22]Physics Department, California Polytechnic State University, San Luis Obispo, CA 93407, USA
[23]INPAC and School of Physics and Astronomy, Shanghai Jiao Tong University; Shanghai Laboratory for Particle Physics and Cosmology, Shanghai 200240, China
[24]Dipartimento di Fisica e Astronomia, Alma Mater Studiorum – Università di Bologna, Bologna I-40127, Italy

Abstract CUORE is a tonne-scale cryogenic experiment located at the Laboratori Nazionali del Gran Sasso that exploits bolometric technique to search for neutrinoless double beta decay of ^{130}Te. Thanks to its very low background and large mass, CUORE is also a powerful tool to study a broad class of phenomena, such as solar axions and WIMP scattering. The ability to conduct such sensitive searches crucially depends on the energy threshold, which has to be kept as low as possible. In this contribution, we show how the trigger algorithm affects the sensitivity to low energy phenomena and the interpretation of the energy spectrum. In particular, we focus on the impact that the trigger algorithm has on the identification of the coincidence events among different crystals and, consequently, on the reconstruction of the background.

Keywords neutrinoless double beta decay · Trigger algorithms · Digital signal processing · Bolometers for dark matter research.

1 CUORE experiment

Neutrinoless double beta decay ($0\nu\beta\beta$, [1]) is a rare, second order nuclear transition in which an initial nucleus (A,Z) decays to a member (A,Z+2) of the same isobaric multiplet with the simultaneous emission of two electrons. In the attempt to investigate the nature of the $0\nu\beta\beta$ various theoretical possibilities were considered, however the general interest has remained focused on the neutrino mass mechanism. $0\nu\beta\beta$ is forbidden by the Standard Model and explicitly violates the lepton number by two units. Its observation would thus prove that the lepton number is not a conserved quantity, and it would also provide us with precious information on the neutrino mass nature and scale. The experimental signature of $0\nu\beta\beta$ is a monoenergetic peak at the Q-value of the decay, considering the summed energy spectrum of the two emitted electrons. The candidate isotopes that could undergo $0\nu\beta\beta$ are even-even nuclei for which single beta decay is energetically forbidden.

The Cryogenic Underground Observatory for Rare Events (CUORE) is an experiment located at the LNGS, Italy, searching for the $0\nu\beta\beta$ of ^{130}Te. This isotope has the highest natural isotopic abundance (34.2%, [2]) among the nuclei of interest. CUORE exploits the bolometric technique to get a high resolution around the $0\nu\beta\beta$ Q-value ($\sim$ 2527.5 keV, [3]). The detector consists of an array of 988 natural-TeO_2 cubic crystals [4], for a total active mass of 742 kg ($\sim$ 206 kg of ^{130}Te).

A bolometer is a sensitive calorimeter that measures the energy deposited by a particle interaction via increase of the temperature of the absorber. Each CUORE bolometer has three fundamental components: an energy absorber,

[25]Service de Physique des Particules, CEA / Saclay, 91191 Gif-sur-Yvette, France
[26]Lawrence Livermore National Laboratory, Livermore, CA 94550, USA
[27]Department of Nuclear Engineering, University of California, Berkeley, CA 94720, USA
[28]INFN – Sezione di Padova, Padova I-35131, Italy
[29]Engineering Division, Lawrence Berkeley National Laboratory, Berkeley, CA 94720, USA

i. e. the crystal itself; a temperature sensor, a neutron-transmutation-doped germanium thermistor that converts the temperature rise into a voltage pulse; and a weak thermal link to the copper frame, which acts both as the structural support and thermal bath to restore the reference temperature. By measuring the signal amplitude we can reconstruct the amount of energy released. At an operating temperature of 10 mK, the typical TeO_2 heat capacity gives a temperature increase of ~ 100 μK per MeV and a signal amplitude of ~ 1 V per MeV. The actual CUORE working temperature is a compromise between a maximal thermal gain and an optimized signal bandwidth.

CUORE is operated at cryogenic temperatures by mean of a powerful custom ^{3}He/^{4}He dilution refrigerator [5]. The dimensions, namely an experimental volume of ~ 1 m^3 and a mass of ~ 17 tonnes, make the CUORE cryostat the largest dilution refrigeration in operation. The cryostat design and construction had to respect very stringent experimental constraints: an effective mechanical insulation, with extremely low vibration levels, and minimal contribution to the radioactive background for the experiment. In particular, in order to suppress the γ and neutron background, two lead shields have been integrated into the cryogenic volume and a lead + polyethylene shield surround the whole cryostat.

The analysis of the data from CUORE-0, a prototype detector equivalent to a single CUORE tower operated as a standalone experiment [6], together with an extensive radio-assay measurement campaign of the materials used for CUORE construction, allowed us to identify the main background sources in the $0\nu\beta\beta$ region of interest (ROI) and to build a Monte Carlo simulation to estimate the expected background index [7]. This is $[1.00 \pm 0.03\ (stat.)\ ^{+0.23}_{-0.10}\ (syst.)]10^{-2}$ counts keV^{-1} kg^{-1} yr^{-1}.

The installation of the CUORE towers inside the cryostat was performed during summer 2016 and we could start the data taking in April 2017.

2 Data processing : Derivative and Optimum trigger

The voltage crossing the thermistor of each bolometer is continuously acquired with a sampling frequency of 1 kHz. A single event is contained in a 10-s window: a 3s-pretrigger gives a measurement of the bolometer temperature, while the 7s-pulse gives the amount energy release, since this is proportional to its amplitude. We also analyze waveforms that do not contain visible pulses to monitor and model our detector noise behaviour. Moreover, each crystal is instrumented with a silicon heater, so that we are able to periodically inject stable voltage pulses with precise and fixed energy in order to correct for possible variation in the detector response.

During the online data acquisition, we save continuous detector waveforms and separately trigger them with a software derivative trigger. This algorithm acts on the rising edge of a pulse: a trigger is fired when the derivative of the pulse stays above a certain threshold for a minimum number of consec-

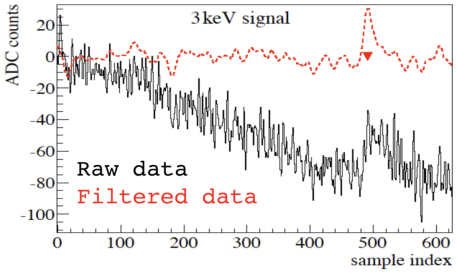

Fig. 1 Window containing a pulse with reconstructed energy of 3 keV. The pulse after the application of the optimum filter is shown in red (Color figure online).

utive samples. This threshold depends on the noise RMS of the individual bolometers.

In order to study low-energy events, we developed an optimum trigger, which runs in parallel to the derivative one [8,9]. We then retriggered all the runs since the beginning of the data taking, using the new algorithm. The optimum trigger is a low threshold trigger based on the optimum filter [10], that maximizes the signal to noise ratio exploiting the distinct power spectra of particle-induced and noise waveforms. Each pulse transfer function is matched to the signal shape so that pulses with a different trend in time are suppressed. We get:

$$H(w_k) \;=\; h\,\frac{s^*(w_k)}{N(w_k)}e^{-jw_k i_M}, \tag{1}$$

where $s(w_k)$ is the discrete Fourier transform of the signal, $N(w_k)$ the noise power spectrum, i_M the position of the maximum of the signal in the acquisition window and h a normalization factor to leave the signal amplitude unchanged. The data buffer is divided into sections that are continuously filtered in the frequency domain with the optimum filter. Once the optimum filter transfer function is built, the baseline is filtered. A trigger threshold, based on the filtered noise RMS, is then applied to properly identify particle events. An example of low-energy event triggered with the optimum trigger is shown in Fig. 1.

2.1 Trigger efficiency evaluation

As a figure of merit for the quality of energy thresholds obtained with a given trigger procedure we use the 90% of the trigger efficiency. We acquire a test run during which we fire multiple heater pulses at different (known) amplitudes on each bolometer. These data are then processed to reconstruct the energy of pulser events that are measured. For each bolometer and each pulser amplitude we compare the number of detected pulser events to the number of events generated. The detection efficiency is estimated as the ratio of the former over the latter. We fit the efficiency as a function of the pulser energy using the

error function (sigmoid shape) and invert it to evaluate the function at the 90% efficiency. This is the value of the energy threshold.

We apply this procedure to both derivative and optimum trigger and then compare the threshold distribution on the whole CUORE detector. In the final steps of the analysis chain (3), in order to select events in the energy spectrum for the $0\nu\beta\beta$ search, we set an analysis threshold common to all bolometers. This choice is specifically meant for the $0\nu\beta\beta$ analysis both with the aim to minimize the background contribution in the region of interest ($\sim$ 55 keV around $Q_{\beta\beta}$) from the 2615 keV ^{208}Tl line, and to ensure that we preserve a trigger efficiency $>$ 90 % for the majority of detectors. The value for this common threshold is 150 keV for derivative trigger (purple line in Fig. 2), and 40 keV with optimum trigger (green line).

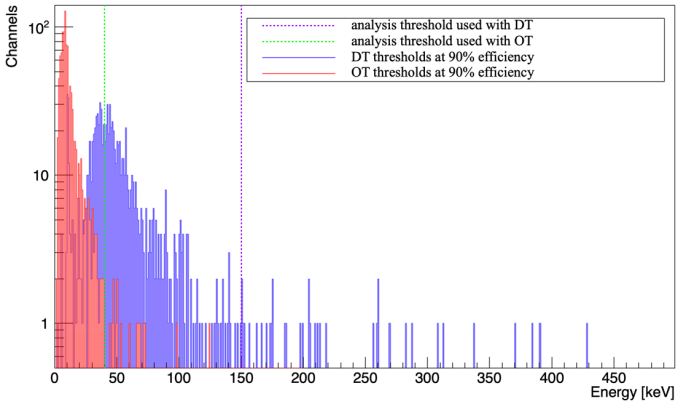

Fig. 2 Distribution of the energy threshold at 90 % detection efficiency. Analysis threshold for both trigger configurations is indicated by the vertical lines (Color figure online).

3 CUORE analysis chain and coincidence identification

The CUORE data analysis consists of a series of following steps, that are performed by using a modular software specifically designed for the experiment.

Initially, the pulse amplitude is estimated by the optimum filter algorithm described in the previous section as the maximum value of the filtered waveform. The signal amplitude is then stabilized against thermal drifts, while the calibration is applied referring to γ lines from ^{232}Th and ^{60}Co sources. Once the energy of physical events is reconstructed, a series of cut is applied to the pulse in order to reliably identify $0\nu\beta\beta$ candidate events. In addition noisy periods of data taking are removed from the analysis and pulses whose shape is not consistent with a true particle-interaction are rejected.

Since we expect from the CUORE Monte Carlo simulations that the largest fraction of the $0\nu\beta\beta$ events ($\sim$88%) will release the whole energy in the same crystal, we apply an anti-coincidence cut that excludes α particles and

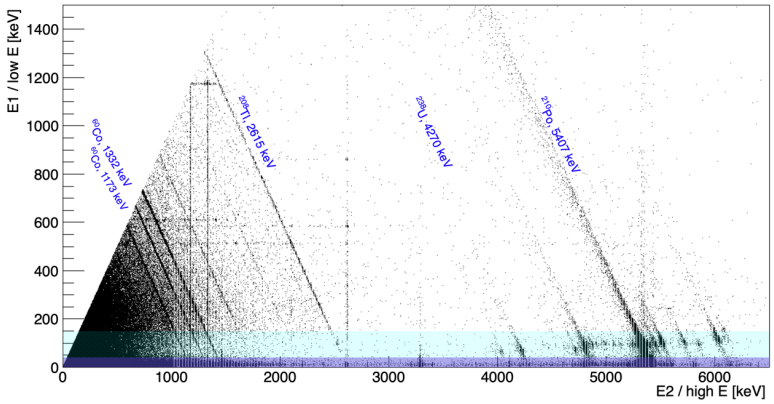

Fig. 3 Multiplicity 2 events scatter plot. $E_1 < E_2$ always. *Light blue* (*blue*) box represents derivative (optimum) trigger analysis threshold. The energy of the main γ and α lines is superimposed. (Color figure online)

multiple-Compton scatterings. We assign a value of *multiplicity*, M, to each event. This parameter indicates the number of crystals interested by the same particle process (within a certain time window). In order to identify the true time difference between two signals, the channels (bolometers) are synchronized using a double correction based both on the time difference between simultaneous events occuring on different towers (i. e. pulser events) and on the intrinsic jitter that exists between physically coincident multi-detector events (e. g. events that sum at 2615 keV, energy of the ^{208}Tl line from the ^{232}Th, during calibration). We set a coincidence window width of 10 ms ($\pm$ 5 ms).

As mentioned in the previous section, lowering the trigger thresholds has an impact on the energy range of particle interactions we can probe. Our capability to detect low energy events considerably increases our efficiency of reconstructing events with energy release in more than one bolometer, i. e. events with multiplicity larger than 1.

Disentangling M_1 and $M_{x\geq 2}$ interactions improves our background reconstruction ability.

Let us focus on the events that populate the M_2 spectrum, referring to Fig. 3. For the purpose of this analysis, we order the energy of coincident events so that, by definition, $E_1 < E_2$, while the derivative and optimum trigger analysis thresholds (150 and 40 keV, respectively) are reported to highlight the energy region that cannot be investigated. As the derivative analysis threshold completely excludes nuclear recoils from α-decay coincidence reconstruction, we will not consider this constrain in the following discussion. Each bolometer will contribute with its own energy threshold, as shown in Sec. 2. The clustering of events along lines with negative slope collect coincident particle events on two bolometers with $E_1 + E_2 = E_{peak}$, where E_{peak} corresponds to a known γ- or α-line, e. g. the ^{208}Tl photopeak. The clustering along ver-

tical lines, i. e. $E_2 = E_{peak}$, while E_1 can have any positive value, correspond to accidental coincidences in most of the cases, that is to say uncorrelated interactions involve different crystals within the same time window. This can interest lines in the spectrum such as the ^{60}Co γs at 1173 and 1332 keV, or the α decays of the ^{238}U and ^{232}Th chains, such as ^{210}Po, that has the highest intensity ($Q_{value} = 5407$ keV).

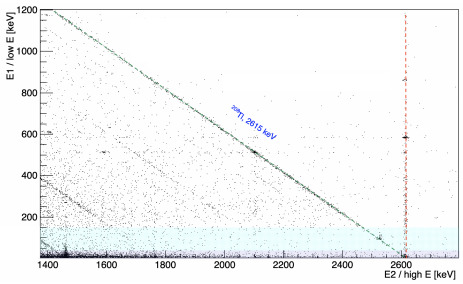

Fig. 4 Zoom around thallium photopeak (2615 keV) of fig. 3. The *green* line represent physical coincidences at 2615 keV ($E_1 + E_2 = 2615$ keV), the *red* one indicates accidental coincidences ($E_2 = 2615$ keV,E_1 any positive value).(Color figure online)

The energy region above the ^{208}Tl line is mainly populated by events originated by contaminants of the TeO_2 crystals (i. e. of the detector itself) and of the detector holder (mostly copper frames). In this region, the dominant background comes from α-decaying isotopes from the ^{238}U and ^{232}Th decay chains. α particles travel extremely short distances inside matter before they are absorbed (a 5 MeV α has a range of about 10 μm in copper), therefore if such an event is seen by the detector, the contaminant has to be in the close proximity of the detector (indeed inside the crystal or the holder surface). If the contaminant is inside the bulk of a crystal, both the α particle and the recoiling nucleus deposit their energy inside it. Such an event has multiplicity 1 and energy equal to the decay Q-value. On the other hand, if the contaminant lies on the crystal surface, the emitted α can leave the crystal. If the same particle is then absorbed by another neighboring crystal, an M_2 event is generated: one crystal triggers on the α particle, the other on the the recoiling nucleus. Events of this kind can be easily identified fixing a constrain on the sum of the energies, that should match the Q_{value} of the decay. They are schematically pictured in Fig. 5. As an example, the raw waveforms of both the α particle and the recoiling nucleus for a typical M_2 event are also shown.

Typically, the nuclear recoil decreases the total energy of the α decay peak by $\sim$ (70 $-$150) keV. This means that the analysis threshold has a strong impact on its detection. Alpha particles and nuclear recoils from the ^{210}Po decay in the M_2 spectrum reconstruction are shown in Fig. 6: while the α particle is detected with both the derivative and optimum trigger analysis, the 150 keV threshold completely prevents the observation of the daughter nuclei events. As a consequence, physical M_2 events wrongly end up in M_1 spectrum.

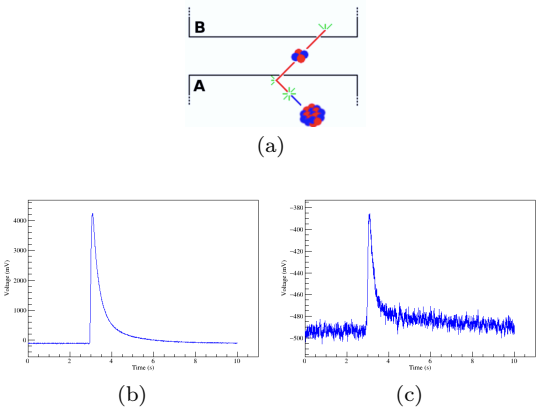

(a) (b) (c)

Fig. 5 (a) is the schematic representation of the processes populating the alpha and recoil peaks in multiplicity 2 spectrum. A and B are two CUORE bolometers. (b) and (c) are the raw pulses of a typical M_2 event coming from alpha decay, (b) is the α particle waveform, (c) the nuclear recoil waveform.

Moving from derivative to optimum trigger analysis, we expect a considerable improvement in our efficiency in M_2 reconstruction, especially in the α region of the spectrum. This is highlighted in Fig. 7. In fact, events in M_1 spectrum move to M_2 when passing from the derivative (*blue*) to optimum (*red*) trigger analysis. Again, we consider the ^{210}Po α particle and compare M_1 and M_2 spectra. To exclude accidentals from the second, we apply an arbitrary cut on the sum of the events energy, i.e. $E_1 + E_2 = Q_{value} \pm \Delta$. Δ is set to 70 keV as it is enough to properly include both the alpha particle and the nuclear recoil events.

It is worth to underline that this analysis was performed with cuts specifically optimized for the $0\nu\beta\beta$ search (2). Using a channel dependent threshold (fig. 2), recoil peaks from surface alpha decays would be visible for a fraction of channels also with the derivative trigger. However, setting a common analysis threshold significantly simplifies the analysis from a technical point of view. Furthermore, having access to the low energy region is helpful both for the background reconstruction and the comprehension of CUORE in general: the spectrum below 40 keV helps us in the reconstruction of X-rays from ^{130}Te and also X-rays from both copper and lead contaminantions [11].

Extending this analysis to other α background sources, we can fix a constraint on the contributions due to contaminants at the crystals surface. This helps us identifying contributions to the α region of the spectrum due to other contaminants, inside the bulk of crystals or at the holder surface. Thus, improving our background model, we can extract with higher accuracy an estimate of our background index in the region of interest for the ^{130}Te $0\nu\beta\beta$.

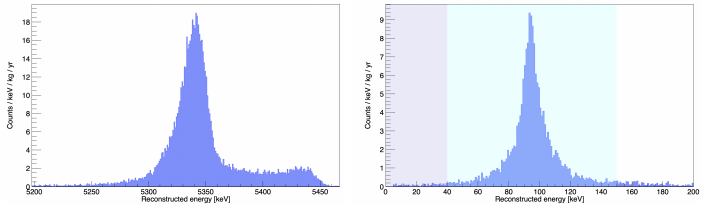

Fig. 6 Alpha particle (*left*) and nuclear recoil (*right*) from ^{210}Po decay. *Light blue* (*blue*) box represents derivative (optimum) trigger analysis threshold.(Color figure online)

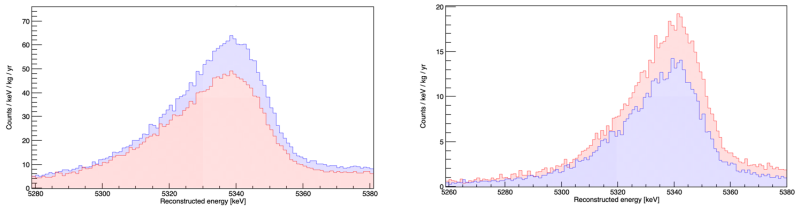

Fig. 7 M_1(*left*) and M_2 (*right*) spectrum comparison in the region of the α particle from ^{210}Po decay. Histograms in *blue* (*red*) are referred to derivative (optimum) trigger analysis. (Color figure online)

4 Conclusions and outlook

The analysis presented shows only a small fraction of the overall improvement we can obtain by using the optimum trigger in the reconstruction of the low-energy spectrum. Besides representing a powerful tool to increase the precision of our background model, the optimum trigger can help us improve the $0\nu\beta\beta$ search by including events in which the electrons release energy in multiple crystals.

References

1. W.H. Furry, Phys. Rev. **56**, 1184 (1939). DOI 10.1103/PhysRev.56.1184
2. M.A. Fehr, M. Rehkamper, A.N. Halliday, Int. J. Mass Spectrometry **232**, 83 (2004). DOI http://dx.doi.org/10.1016/j.ijms.2003.11.006
3. D.A. Nesterenko, K. Blaum, M. Block, C. Droese, S. Eliseev, F. Herfurth, et al., Phys. Rev. C **86**, 044313 (2012). DOI 10.1103/PhysRevC.86.044313
4. C. Alduino, et al., J. Instrum. **11**(07), P07009 (2016). DOI 10.1088/1748-0221/11/07/P07009
5. C. Alduino, et al., Cryogenics **102**, 9 (2019). DOI 10.1016/j.cryogenics.2019.06.011
6. K. Alfonso, et al., Phys. Rev. Lett. **115**(10), 102502 (2015). DOI 10.1103/PhysRevLett.115.102502
7. C. Alduino, et al., Eur. Phys. J. C **77**(8), 543 (2017). DOI 10.1140/epjc/s10052-017-5080-6
8. S. Di Domizio, F. Orio, M. Vignati, J. Instrum. **6**, P02007 (2011). DOI 10.1088/1748-0221/6/02/P02007
9. C. Alduino, et al., Eur. Phys. J. C **77**(12), 857 (2017). DOI 10.1140/epjc/s10052-017-5433-1
10. E. Gatti, P.F. Manfredi, Riv. Nuovo Cim. **9**, 1 (1986). DOI 10.1007/BF02822156
11. http://nucleardata.nuclear.lu.se/toi/